Hepatocellular Carcinoma: Intra-arterial Delivery of Doxorubicin-loaded Hollow Gold Nanospheres for Photothermal Ablation—Chemoembolization Therapy in Rats[1]

Junjie Li, PhD
Min Zhou, PhD
Fengyong Liu, MD[2]
Chiyi Xiong, PhD
Wanqin Wang, MD[3]
Qizhen Cao, PhD
Xiaoxia Wen, MS
J. David Robertson, PhD
Xin Ji, PhD
Y. Andrew Wang, PhD
Sanjay Gupta, PhD
Chun Li, PhD

Purpose: To determine if combretastatin A-4 phosphate disodium (CA4P) can enhance the tumor uptake of doxorubicin (Dox)-loaded, polyethylene glycol (PEG)–coated hollow gold nanospheres (HAuNS) mixed with ethiodized oil for improved photothermal ablation (PTA)–chemoembolization therapy (CET) of hepatocellular carcinoma (HCC) in rats.

Materials and Methods: Animal experiments were approved by the institutional animal care and use committee and performed from February 2014 to April 2015. Male Sprague-Dawley rats (n = 45; age, 12 weeks) were inoculated with N1S1 HCC cells in the liver, and 8 days later, were randomly divided into two groups of 10 rats. Group 1 rats received intrahepatic arterial injection of PEG-HAuNS and ethiodized oil alone; group 2 received pretreatment with CA4P and injection of PEG-HAuNS and ethiodized oil 5 minutes later. The gold content of tumor and liver tissue at 1 hour or 24 hours after injection was quantified by using neutron activation analysis (n = 5 per time point). Five rats received pretreatment CA4P, PEG-copper 64-HAuNS, and ethiodized oil and underwent micro–positron emission tomography (PET)/computed tomography (CT). In a separate study, three groups of six rats with HCC were injected with saline solution (control group); CA4P, Dox-loaded PEG-coated HAuNS (Dox@PEG-HAuNS), and ethiodized oil (CET group); or CA4P, Dox@PEG-HAuNS, ethiodized oil, and near-infrared irradiation (PTA-CET group). Temperature was recorded during laser irradiation. Findings were verified at postmortem histopathologic and/or autoradiographic examination. Wilcoxon rank-sum test and Pearson correlation analyses were performed.

Results: PEG-HAuNS uptake in CA4P-pretreated HCC tumors was significantly higher than that in non–CA4P-pretreated tumors at both 1 hour ($P < .03$) and 24 hours ($P < .01$). Mean ± standard deviation of tumor-to-liver PEG-HAuNS uptake ratios at 1 hour and 24 hours, respectively, were 5.63 ± 3.09 and 1.68 ± 0.77 in the CA4P-treated group and 1.29 ± 2.40 and 0.14 ± 0.11 in the non–CA4P-treated group. Micro-PET/CT allowed clear delineation of tumors, enabling quantitative imaging analysis. Laser irradiation increased temperature to 60°C and 43°C in the tumor and adjacent liver, respectively. Mean HCC tumor volumes 10 days after therapy were 1.68 cm^3 ± 1.01, 3.96 cm^3 ± 1.75, and 6.13 cm^3 ± 2.27 in the PTA-CET, CET, and control groups, respectively, with significant differences between the PTA-CET group and other groups ($P < .05$).

Conclusion: CA4P pretreatment caused a higher concentration of Dox@PEG-HAuNS to be trapped inside the tumor, thereby enhancing the efficacy of anti–HCC treatment with PTA-CET in rats.

Online supplemental material is available for this article.

[1] From the Departments of Cancer Systems Imaging (J.L., M.Z., C.X., W.W., Q.C., X.W., C.L.) and Interventional Radiology (F.L., S.G.), the University of Texas MD Anderson Cancer Center, Houston, 1515 Holcombe Blvd, TX 77030; Department of Chemistry, University of Missouri, Columbia, Mo (J.D.R.); and Ocean Nanotech, San Diego, Calif (X.J., Y.A.W.). Received November 13, 2015; revision requested January 4, 2016; revision received March 16; accepted April 8; final version accepted April 15. **Address correspondence to** C.L. (e-mail: *cli@mdanderson.org*).

J.L. supported in part by the Odyssey Program and H-E-B Award for Scientific Achievement at MD Anderson Cancer Center, study supported by the National Institutes of Health (grant R44 CA196025) and by the John S. Dunn Foundation. Research animal support facility and small animal imaging facility supported by a Cancer Center Support Grant from the National Institutes of Health (P30CA016672).

Current addresses:
[2] Department of Interventional Radiology, Chinese PLA General Hospital, Beijing, P.R. China.
[3] Department of Radiology, the First Affiliated Hospital of Anhui Medical University, Anhui, P.R. China.

Conventional chemotherapy and radiation therapy have limited efficacy against hepatocellular carcinoma (HCC). Few patients meet the criteria for surgical resection and liver transplantation because of their existing intrinsic liver disease or a scarcity of donor livers (1,2). Minimally invasive imaging-guided interventional techniques including transarterial and percutaneous interventions (eg, radiofrequency ablation, laser ablation) also are limited by frequent local tumor recurrence due to incomplete elimination of cancer cells. New multimodal therapies are needed to improve tumor response and prolong survival in patients with HCC.

Photothermal conversion nanoparticles such as hollow gold nanospheres (HAuNS) have strong absorption that is tunable in the near-infrared region and capable of converting the absorbed photographic energy into heat for photothermal ablation (PTA) of tumor cells. Doxorubicin (Dox)-loaded, polyethylene glycol (PEG)–coated HAuNS (Dox@PEG-HAuNS) can be used with near-infrared laser irradiation to mediate simultaneous PTA and chemoembolization therapy (CET) of cancer cells. Near-infrared laser irradiation both elevates the temperature of the treated tissue and destroys it, triggering the nanospheres to release their cytotoxic Dox payload directly into the tumor (3–5). The low systemic toxicity and superior antitumor efficacy of this combined approach have been demonstrated in ectopic human tumor xenografts after intravenous injection of either targeted or nontargeted nanoparticles (4,5). However, these approaches have not been adapted for the treatment of HCC because of substantial uptake of Dox@PEG-HAuNS in normal liver tissue. Although intrahepatic arterial injection with an embolic agent, ethiodized oil, has been used for selective delivery of high doses of small–molecular-weight therapeutic agents to tumors (6), to our knowledge, the delivery of nanoparticles such as Dox@PEG-HAuNS and ethiodized oil via the intrahepatic arterial route in rat models of HCC has not been demonstrated.

A high tumor-to-liver uptake ratio of nanoparticles ensures an improved therapeutic index while minimizing systemic adverse effects and reducing potential damage to surrounding tissue. However, there are several obstacles to achieving high tumor-to-liver uptake ratios of nanoparticles such as PEG-HAuNS. Limited interstitial fluid flow, vessel permeability, and the leaky space in tumors restrict the penetration and deposition of nanoparticles into the tumor interstitial space (7). In addition, most nanoparticles are taken up by the Kupffer cells of the reticuloendothelial system in the liver (8). Nanoparticle size restricts their extravasation into the extravascular extracellular space (9). Finally, blood perfusion may facilitate the subsequent wash-out of nanoparticles from the tumor after saturation. The resulting heterogeneous deposition of nanoparticles inside the tumor may compromise their therapeutic effect.

Vascular disrupting agents, which have been studied extensively in the development of new antitumor agents (10), may provide a means of overcoming these obstacles. Tubulin-binding vascular disrupting agents selectively bind to microtubules in the endothelial cells of tumor vessels, causing potent disruption of the cytoskeleton and morphologic changes in endothelial cells (11). The nearly instantaneous increase in vascular permeability promotes the excess extravasation of plasma macromolecules into the extravascular extracellular space; consequently, blood flow resistance increases and vascularity collapses within hours after injection of the vascular disrupting agent (12,13). Thus, pretreating tumors with potent vascular disrupting agents such as combretastatin A-4 phosphate disodium (CA4P) (13) may improve tumor uptake and retention of PEG-HAuNS by increasing vessel permeability to allow more PEG-HAuNS to extravasate into the tumor and collapsing blood vessels to limit perfusion, hence trapping PEG-HAuNS with prolonged retention. The

Advances in Knowledge

- The disruption of hepatocellular carcinoma tumor vessels enhanced tumor uptake and retention of intrahepatic arterially injected nanoparticles in rats, as shown by the significant increase in tumor-to-liver uptake ratios from 1.29 ± 2.40 to 5.63 ± 3.09 at 1 hour and from 0.14 ± 0.11 to 1.68 ± 0.77 at 24 hours after injection.
- Combined photothermal ablation–chemoembolization therapy mediated by multifunctional doxorubicin-loaded, polyethylene glycol–coated hollow gold nanospheres mixed with ethiodized oil resulted in a significant improvement in antitumor effects compared with chemoembolization therapy alone (mean tumor volume 10 days after therapy, 1.68 cm^3 ± 1.01 and 3.96 cm^3 ± 1.75, respectively; $P < .05$).

Implication for Patient Care

- The proposed treatment approach is potentially useful for the treatment of patients with unresectable locally advanced hepatocellular carcinoma.

Published online before print
10.1148/radiol.2016152510 **Content codes:** GI MI

Radiology 2016; 281:427–435

Abbreviations:
CA4P = combretastatin A-4 phosphate disodium
CET = chemoembolization therapy
Dox = doxorubicin
Dox@PEG-HAuNS = Dox-loaded PEG-coated HAuNS
HAuNS = hollow gold nanospheres
HCC = hepatocellular carcinoma
PEG = polyethylene glycol
PTA = photothermal ablation

Author contributions:
Guarantors of integrity of entire study, J.L., F.L., Y.A.W., C.L.; study concepts/study design or data acquisition or data analysis/interpretation, all authors; manuscript drafting or manuscript revision for important intellectual content, all authors; approval of final version of submitted manuscript, all authors; agrees to ensure any questions related to the work are appropriately resolved, all authors; literature research, J.L., F.L., X.J., C.L.; clinical studies, J.L., F.L.; experimental studies, J.L., M.Z., F.L., C.X., W.W., Q.C., X.W., J.D.R., X.J., Y.A.W., C.L.; statistical analysis, J.L., F.L., C.L.; and manuscript editing, J.L., F.L., J.D.R., S.G., C.L.

Conflicts of interest are listed at the end of this article.

goal of this study was to determine if CA4P can enhance the tumor uptake of Dox@PEG-HAuNS and ethiodized oil for improved PTA-CET of HCC in rats.

Materials and Methods

PEG-HAuNS were either synthesized in house or provided by Ocean Nanotech (San Diego, Calif), which is the employer of two of the authors (J.X. and W.A.) of this study. The authors who are not employees of Ocean Nanotech had control of inclusion of any data and information that might present a conflict of interest for those authors who are employed by Ocean Nanotech. Synthesis and characterization of PEG-HAuNS and Dox@PEG-HAuNS as well as copper 64 (^{64}Cu) radiolabeling (M.Z., a chemist with 7 years of experience) are described in Appendix E1 (online).

Tumor Inoculation

The N1S1 rat hepatoma cell line (Obtained from Rony Avritscher, MD; MD Anderson Cancer Center) was cultured in Iscove's modified Dulbecco's medium (ATCC, Manassas, Va) supplemented with 10% fetal bovine serum and 1% penicillin–streptomycin and incubated at 37°C in a humidified 5% carbon dioxide atmosphere. Cells were maintained in suspension in 75-cm^2 culture flasks. All animal experiments were approved by the institutional animal care and use committee. Animal studies were performed in 45 male Sprague-Dawley rats (age, 12 weeks; weight range, 340–380 g; Harlan Laboratories, Indianapolis, Ind) from February 2014 to April 2015. Rats were anesthetized with an intraperitoneal injection of 60 mg/kg of pentobarbital. After the abdomen of each rat was shaved and prepared for aseptic surgery, a 2-cm vertical midline laparotomy was performed, and the left liver lobe was exposed. N1S1 cells (7×10^6) in 50 μL of phosphate-buffered saline solution mixed with a solubilized basement membrane preparation (in a 1:1 ratio) extracted from the Engelbreth-Holm-Swarm mouse sarcoma (Matrigel; Corning Life Sciences, Corning, NY) were injected into the liver. The abdominal cavity was then closed in two layers with 3.0 silk sutures. All experiments were started on day 8, after tumors had grown to a mean ± standard deviation diameter of 8 mm ± 3.

Intrahepatic Arterial Cannulation

The gastroduodenal artery was isolated with two 6.0 sutures, and the tip of a 2F silicone microcatheter (Access Technologies, Skokie, Ill) was advanced through an arterial incision made between the two sutures to the proper hepatic artery, and the artery was ligated with a slipknot from both sides to fix the catheter. Injections were given by using an infusion pump at a rate of 6 mL per hour. The catheter was then carefully withdrawn from the arterial incision ile the suture was gently tightened to prevent bleeding. The gastroduodenal artery was then permanently ligated, and the abdominal cavity was sutured in two layers (J.L., with 8 years of experience in interventional procedures). Two rats in which intrahepatic arterial injection was unsuccessful were excluded from subsequent experiments.

PEG-HAuNS Trapping Effect by CA4P

Two groups of 10 HCC–bearing rats each received intrahepatic arterial injection of either PEG-HAuNS and ethiodized oil alone (0.25 mL/kg of 20 optical density PEG-HAuNS [0.5 mg/mL], mixed with 50 μL of ethiodized oil) or CA4P (15 mg/kg) followed by PEG-HAuNS and ethiodized oil 5 minutes later (Fig 1). Five rats per group underwent micro–computed tomography (micro-CT) at either 1 hour only or at both 1 hour and 24 hours after PEG-HAuNS and ethiodized oil injection. Immediately after micro-CT, the rats were killed by means of carbon dioxide inhalation. Tumors and adjacent normal liver tissue samples were excised and divided; one-half of each sample was used for quantification of gold content, and the other was used for histopathologic examination.

Quantification of Gold Content

Gold content in the liver and tumor samples was analyzed by means of neutron activation analysis as described previously (16).

Micro-PET/CT

Five rats received intrahepatic arterial injection of CA4P (15 mg/kg in 100 μL of phosphate-buffered saline solution) followed by PEG-(^{64}Cu)-HAuNS and ethiodized oil (7.4 MBq, 0.25 mL/kg of 20 optical density PEG-HAuNS [0.5 mg/mL] and 50 μL of ethiodized oil) 5 minutes later. One hour after injection, the rats were given isoflurane gas anesthesia and were imaged with a small animal micro-PET/CT scanner (Inveon; Siemens Preclinical Solutions, Knoxville, Tenn) (Fig 1). Acquisition parameters are listed in the Table. Micro-CT and micro-PET images from the same scan were fused by using the Inveon research workplace (Siemens). Regions of interest were drawn manually around whole tumors on micro-CT images and were copied to the corresponding micro-PET images. In a similar way, circular regions of interest were drawn on livers on micro-CT images and copied to the corresponding micro-PET images (J.L., with 8 years of experience in imaging acquisition and data analysis). The CT numbers in Hounsfield units from micro-CT and/or the signal intensity values from micro-PET were used to calculate the tumor-to-liver uptake ratios.

PEG-(^{64}Cu)-HAuNS Biodistribution

After micro-PET/CT, the rats were killed and major organs were removed and weighed, and their radioactivity was measured with a gamma counter (Packard Cobra; GMI, Ramsey, Minn). Excised tumors were divided; one-half were used for radioactivity assessment, and the other were used for autoradiographic and histologic examination. Radioactivity was expressed as the percentage of the injected dose per gram of tissue.

Autoradiography

Tumors and surrounding normal liver specimens collected after micro-PET/CT were snap-frozen with optimum–cutting-temperature compound (Sakura Finetek) and sliced into three consecutive 10-μm sections at 20°C by using a research cryostat (CM3050 S; Leica, Wetzlar, Germany). The tissue sections

Figure 1

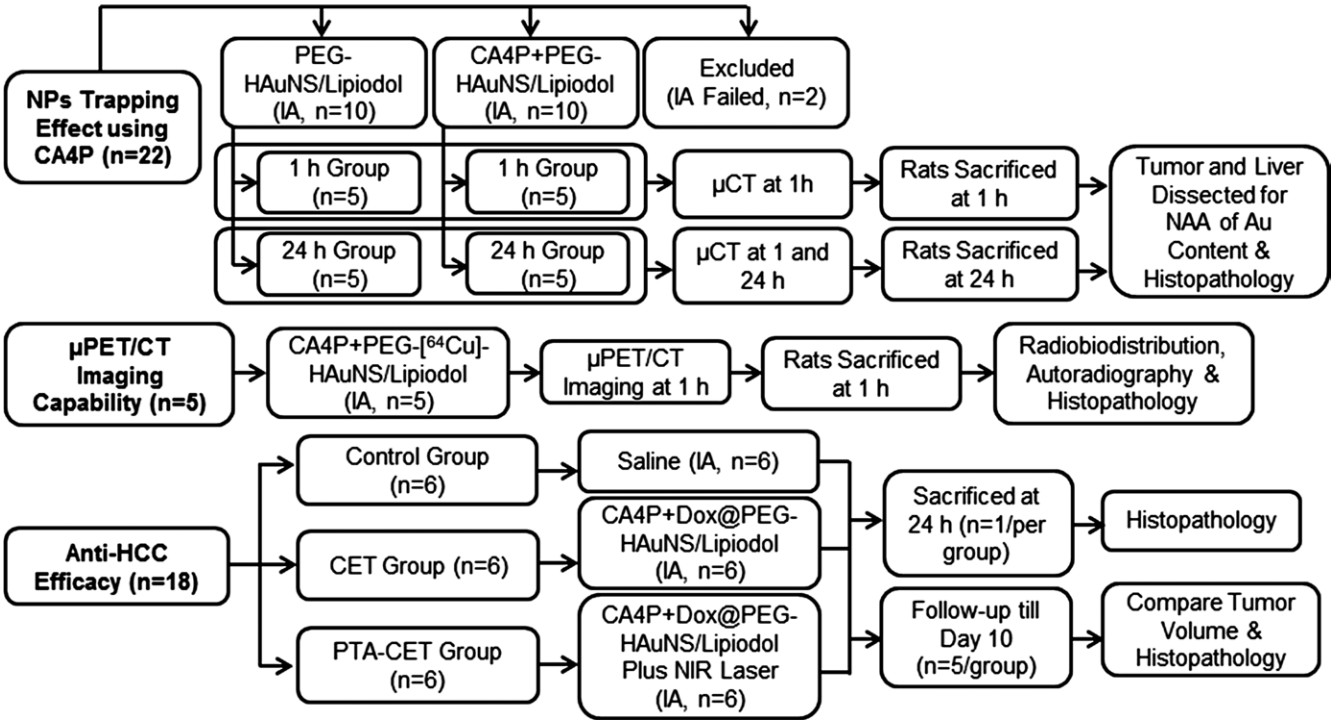

Figure 1: Flow diagram shows rats bearing orthotopic HCC. *IA* = intrahepatic arterial injection, *Au* = gold, *NAA* = neutron activation analysis, *NIR* = near infrared, *NP* = nanoparticle, *μCT* = micro-CT, *μPET* = micro-PET.

were thaw-mounted on glass slides and allowed to air dry. The sections were then exposed to BAS-SR 2025 phosphorous film for 24 hours. The film was scanned with a multifunctional imaging system (FLA5100 Multifunctional Imaging System; Fujifilm Medical Systems, Stamford, Conn). After film exposure, the frozen sections were stained with hematoxylin and eosin for confirmation of findings from biodistribution and micro-PET/CT imaging.

Anti-HCC Efficacy

In a separate study, treatment responses were compared among three groups of six rats that received intrahepatic arterial injections of one of three solutions or combinations of solutions 1 hour after injection: *(a)* saline solution (control group), *(b)* CA4P (15 mg/kg) and Dox@PEG-HAuNS (0.4 mg/mL Dox; 0.5 mg/mL 20 optical density PEG-HAuNS) and 50 μL of ethiodized oil (CET group), or *(c)* CA4P, Dox@PEG-HAuNS, ethiodized oil, and near-infrared laser irradiation (laser wavelength, 808 nm; power density, 4 W/cm^2; two treatments at 2 minutes per treatment [PTA-CET group]; Fig 1). Tissue temperatures during near-infrared irradiation were measured every 10 seconds by using a thermal camera (Flir i7; Flir Systems, Portland, Ore). One rat from each group was killed 24 hours after injection, and its tumor and liver were resected for fluorescence microscopic analysis to verify the release and intratumoral distribution of Dox. The remaining five rats in each group, whose health and body weight were monitored daily, were killed 10 days after treatment, and their tumors were excised, weighed, and then cryosectioned for histologic evaluation.

Histopathologic Evaluation

A fluorescence microscope (Axio Observer.Z1; Carl Zeiss MicroImaging, Jena, Germany) was used (magnification, ×100) to examine the hematoxylin and eosin–stained sections (J.L., with 8 years of experience in histopathology). The scattering signal intensity from PEG-HAuNS was visualized by using a dark-field condenser, and Dox was visualized by using fluorescence microscopy at excitation and emission wavelengths of 488 nm and 565 nm, respectively.

Statistical Analysis

Differences between groups were analyzed by using the Wilcoxon rank-sum test, and *P* values were considered to indicate a significant difference at less than or equal to .05. Pearson correlation analyses were performed to evaluate the correlation between the gold content quantified from neutron activation analysis and the CT numbers in Hounsfield units from CT imaging (n = 15). The sample size and distribution met the normality assumption. Statistical analysis was performed by using software (Prism 6; GraphPad, La Jolla, Calif).

Micro-CT/PET Parameters

Modality and Parameter	Value
Micro-CT	
Total rotation (degrees)	360
No. of rotation steps	180
No. of calibrations	20
Charge-coupled device readout (pixels)	
Transaxial	2048
Axial	3072
No. of bins	4
Exposure time (msec)	330
Effective pixel size (μm)	112.48
Field of view (mm)	
Transaxial	57.59
Axial	86.38
Multibed no.	2
Field of view overlap (%)	20
Micro-PET	
Acquisition time (sec)	300
Photopeak energy level (KeV)	511
Lower level discrimination (KeV)	350
Upper level discrimination (KeV)	650
Timing window (nsec)	3432

Figure 2

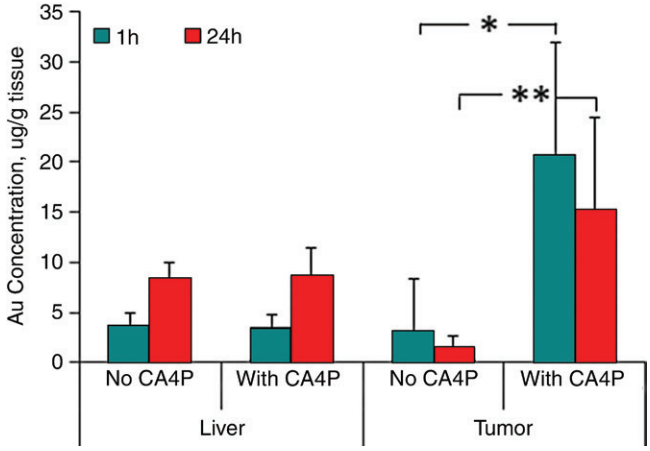

Figure 2: Bar graph shows neutron activation analysis of gold *(Au)* content. *Au* concentrations (in micrograms per gram of tissue) in tumor and liver tissue were measured at 1 hour and 24 hours after intrahepatic arterial injection of PEG-HAuNS with or without CA4P pretreatment. *Au* concentrations in the CA4P-treated tumors were significantly higher than those in the non–CA4P-treated tumors at both 1 hour (* = $P < .03$; ** = $P < .01$) and 24 hours after PEG-HAuNS injection.

Results

All rats survived anesthesia, surgical procedures, and laser treatment. No rats had excessive bleeding or substantial weight loss. All rats had developed tumors at 8 days after inoculation, a rate higher than those reported previously (17). Micro-CT revealed that 43 of 45 (96%) intrahepatic arterial injections were successful.

Quantification of Gold Concentration by Means of Neutron Activation Analysis and Micro-CT

Neutron activation analysis of gold concentration revealed that the mean PEG-HAuNS uptake at 1 hour and 24 hours was 20.72 μg/g ± 11.21 (range, 9.95–37.98 μg/g) and 15.19 μg/g ± 9.22 (range, 6.25–25.47 μg/g), respectively, in the CA4P-treated tumor, and 3.18 μg/g ± 5.22 (range, 0.52–12.51 μg/g) and 1.46 μg/g ± 1.26 (range, 0.23–3.35 μg/g), respectively, in the non–CA4P-pretreated tumors. PEG-HAuNS uptake in CA4P-treated tumors was significantly higher than that in the non–CA4P-pretreated tumors at both 1 hour ($P < .03$) and 24 hours ($P < .01$; Fig 2). The mean gold concentration in the CA4P- and non–CA4P-pretreated tumors 24 hours after injection were 73.3% and 45.9%, respectively, of those in the tumors 1 hour after injection (Fig E1 [online]). The liver uptake of PEG-HAuNS in the CA4P- and non–CA4P-pretreated groups was 3.56 ± 1.32 (range, 2.24–5.46) and 3.53 ± 1.23 (range, 2.67–5.50), respectively at 1 hour, and 8.33 ± 1.68 (range, 6.04–10.50) and 8.75 ± 2.64 (range, 4.95–11.27), respectively, at 24 hours; which did not differ significantly at either 1 hour or 24 hours. Regardless of CA4P use, the liver uptake of PEG-HAuNS at 24 hours was significantly higher than that at 1 hour ($P < .01$; Fig 2). Rats in the CA4P-pretreated group at 1 hour had the highest tumor-to-liver PEG-HAuNS uptake ratio (5.63 ± 3.09; range, 2.50–9.66).

PEG-HAuNS and ethiodized oil allowed the high-contrast delineation of both CA4P- and non–CA4P-pretreated tumors by means of micro-CT at 1 hour. But at 24 hours, the contrast enhancement of the CA4P-pretreated tumors was moderately decreased, and that of the non–CA4P-pretreated tumors was almost completely eliminated (Fig 3). The CT numbers of the tumors on the micro-CT images and the corresponding gold concentrations obtained from neutron activation analysis had a strong positive linear correlation ($y = 14.3x + 93.84$, $r^2 = 0.95$; 95% confidence interval: 12.01, 16.05; Fig E2 [online]).

Histopathologic Analysis

Representative photomicrographs of the tumor and liver sections are shown (Fig 4). PEG-HAuNS were widely dispersed in the macrophages and extracellular and intravascular spaces of the liver at 1 hour and 24 hours but were much more prevalent at 24 hours than at 1 hour. In non–CA4P-pretreated tumors, PEG-HAuNS were clustered mainly inside or around the blood vessels; much fewer PEG-HAuNS were in the tumor interstitium, and tumor cells appeared viable, without massive tumor necrosis. In CA4P-pretreated tumors, PEG-HAuNS were widely dispersed, with extensive hemorrhage and cell death inside the tumor, presumably due to the vascular disrupting effect of

Figure 3

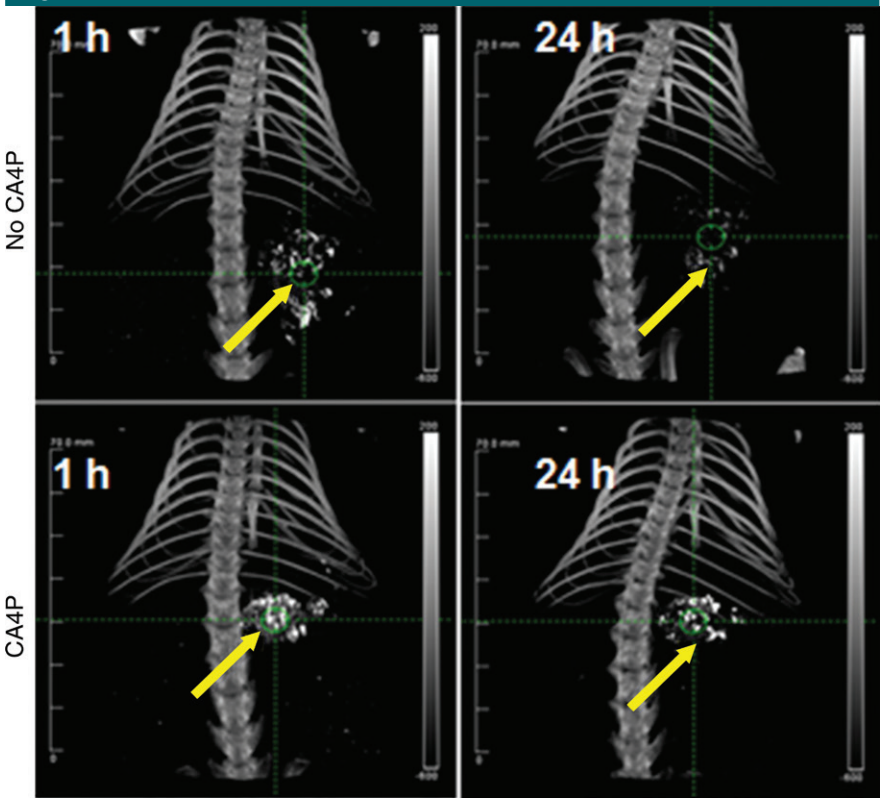

Figure 3: Representative micro-CT images show tumors (arrows) at 1 hour and 24 hours after intrahepatic arterial injection of PEG-HAuNS and ethiodized oil with and without CA4P pretreatment.

CA4P. Dark-field imaging revealed that the tumor distribution of PEG-HAuNS in the CA4P-pretreated group was more homogeneous than that in the non–CA4P-pretreated group. Gross sections of CA4P-pretreated tumors were gold colored, whereas those of non–CA4P-treated tumors were whitish, indicating that CA4P-pretreated tumors had more PEG-HAuNS.

Micro-PET/CT, Histopathologic, Autoradiographic, and Biodistribution Results

In agreement with the findings of the neutron activation analysis and micro-CT studies, micro-PET images acquired 1 hour after intrahepatic arterial injection of PEG-(^{64}Cu)-HAuNS and ethiodized oil showed the highest accumulation of the nanoparticles in the tumor, which colocalized with the tumors delineated at micro-CT (Fig 5, *A*). The micro-PET–measured tumor-to-liver activity ratio was 5.43 ± 2.79, which was in line with that of the neutron activation analysis method. The highest activity areas on the autoradiographs matched the tumor areas in the corresponding hematoxylin and eosin–stained sections (Fig 5, *B*). Ex vivo tissue biodistribution analysis revealed that the tumor had the highest radioactivity, whereas the liver had relatively low radioactivity. The small intestine and kidneys had moderate radioactivity; the lung, spleen, and stomach also had relatively low radioactivity; and the blood, brain, heart, large intestine, skin, muscle, and bone had the lowest radioactivity (Fig 5, *C*).

Therapeutic Efficacy with Dox@PEG-HAuNS

The intrahepatic arterial procedure and/or near-infrared irradiation elicited an acute adverse effect in all rats within 2–3 days, as shown in hair loss, appetite loss, reduced activity, and slightly reduced body weight (< 4%). The rats' body weights recovered throughout the remaining 10-day study period. During near-infrared irradiation, temperatures in the tumor region increased rapidly to approximately 60°C within 90 seconds and remained at this level until irradiation was stopped. The temperature of adjacent normal liver tissue increased slightly, to approximately 43°C. Temperatures in distant liver tissue remained unchanged (Fig E3 [online]).

In the PTA-CET rats, the accumulation of Dox@PEG-HAuNS in the necrotic tumor area 24 hours after near-infrared irradiation overlapped with the fluorescence signal from Dox, indicating that near-infrared irradiation triggered the release of Dox from Dox@PEG-HAuNS. The tumor area had extensive cell death, whereas the adjacent nontumorous hepatic tissue was typically composed of intact hepatocytes with normal, clear cytoplasm and no nuclear atypia or mitoses (Fig E4 [online]). Mean tumor volumes measured with calipers were 1.54 cm^3 ± 0.29 (range, 1.07–2.03 cm^3) at the time of intrahepatic arterial injection, with no significant differences among groups. However, 10 days after treatment, tumor volumes were 1.68 cm^3 ± 1.01 (range, 0.32–2.93 cm^3), 3.96 cm^3 ± 1.75 (range, 2.52–6.99 cm^3), and 6.13 cm^3 ± 2.27 (range, 2.89–8.67 cm^3) in the PTA-CET, CET, and control groups, respectively, and differed significantly between the PTA-CET group and the other two groups ($P < .05$), but not between the CET group and the control group ($P = .13$) (Fig 6).

Histopathologic analysis revealed that tumors in the PTA-CET group had extensive central necrosis surrounded by a rim of inflammatory cells, adhesive normal cells, and a few viable tumor cells. Treatment with CA4P plus Dox@PEG-HAuNS and ethiodized oil but without near-infrared irradiation also induced necrosis, albeit to a lesser extent. CET-group tumors had less central necrosis than did PTA-CET group tumors, with scattered peripheral necrosis surrounded by inflammatory cells and thick viable tumor cells. Control group tumors had irregular

Figure 4

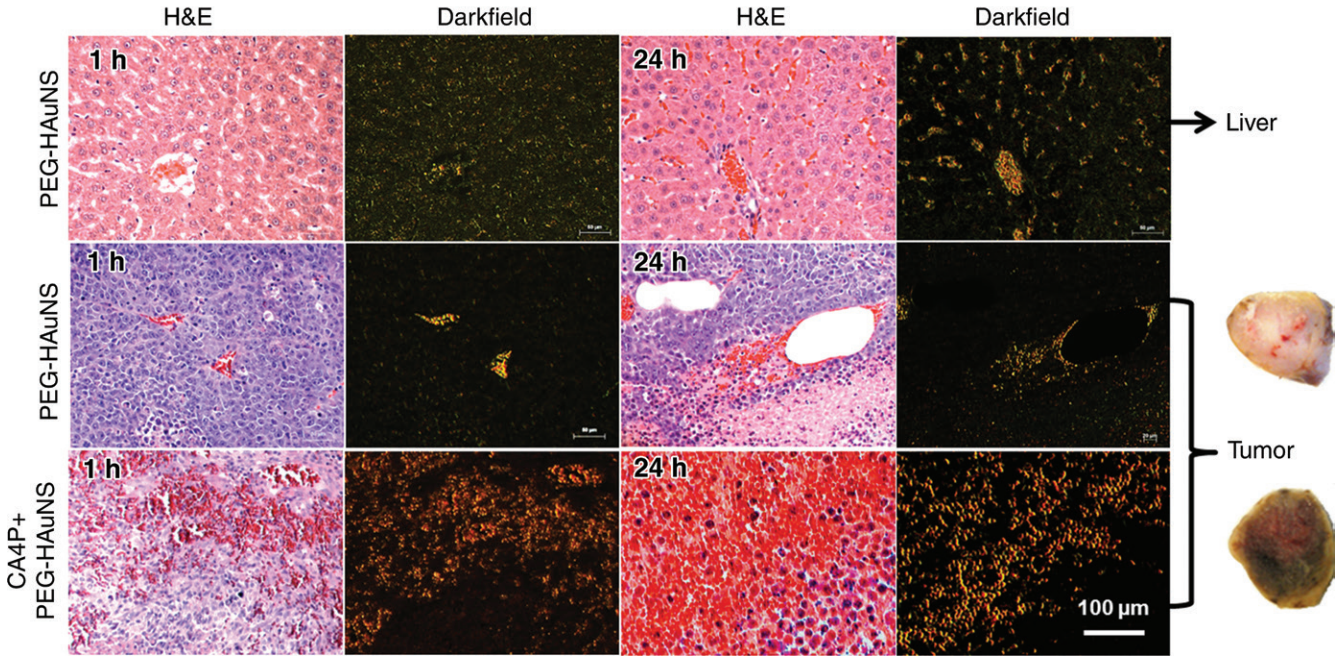

Figure 4: Representative microphotographs of N1S1 tumors and adjacent normal liver tissue from rats that received intrahepatic arterial injections of PEG-HAuNS and ethiodized oil with or without CA4P pretreatment. Tissue sections were stained with hematoxylin and eosin (*H & E*). Dark-field microscopy revealed PEG-HAuNS. In normal liver (top), PEG-HAuNS accumulated in either Kupffer cells or the intercellular space in liver parenchyma, and this accumulation was higher at 24 hours than at 1 hour after injection of PEG-HAuNS. In non–CA4p-pretreated tumors (middle), only a few PEG-HAuNS were clustered in the tumor vessels or in the extravascular space surrounding the blood vessels, and few PEG-HAuNS were in the tumor interstitial space. In comparison, the CA4P-pretreated tumors (bottom) show extensive hemorrhagic necrosis accompanied by large amount of PEG-HAuNS. Gross sections of CA4P-treated tumors were goldish, indicating accumulation of PEG-HAuNS, whereas those of non–CA4P-treated tumors were pale (representative gross sections are shown).

spontaneous necrosis surrounded by viable tumor cells (Fig E5 [online]).

Discussion

Our findings suggest that CA4P pretreatment improves tumor uptake and retention of Dox@PEG-HAuNS and thus brings better antitumor efficacy of PTA-CET capable of micro-PET/CT imaging and quantification. HCCs are generally hypervascular and contain intensive neovascularity suitable for treatment with vascular disrupting agents. CA4P induces necrosis in central tumor cells but not peripheral tumor cells, which are nourished by blood from adjacent normal tissue and survive and repopulate rapidly (18). CA4P has been used with chemotherapy, radiation therapy, and/or hyperthermia against a range of tumor types in clinical trials (19,20). The schedule, sequence, and timing of vascular disrupting agents and combination therapies are crucial in determining the antitumor efficacy of the combination therapy because of vascular disrupting agents' prominent effect on tumor vasculature (21). Martinelli et al (21) suggested that chemotherapy should be given 72 hours after injection of vascular disrupting agents. Wang et al (22) proposed giving vascular disrupting agents 1–4 hours before administering chemotherapeutic drugs.

The potential correlation of vascular disrupting agent–induced changes in tumor vascularity and blood biomarkers has been studied extensively. Tozer et al (23) reported that the vasculature permeability of P22 rat carcinosarcomas increased 160% within 10 minutes of injection of 100 mg/kg of CA4P; 1 hour after injection, tumor blood flow was less than 5% of the starting value. Extensive tumor microvasculature destruction occurred within 1 hour of CA4P administration (23,24). Li et al (25) showed that necrosis-avid iodine 123–hypericin and Evans Blue stain intravenously injected 24 hours after CA4P were prevented from entering the tumor core of rhabdomyosarcomas in rat livers. CA4P's trapping effect with improved retention of contrast agent in the tumor has been quantitatively analyzed at dynamic contrast material–enhanced magnetic resonance imaging (26).

We found that CA4P induced a PEG-HAuNS–trapping effect in HCC tumors. Compared with non–CA4P-pretreated tumors, CA4P-pretreated tumors had significantly enhanced early uptake (at 1 hour) and prolonged retention (at 24 hours) of PEG-HAuNS. The strong positive linear correlation between the CT numbers of the tumors on the micro-CT images and the corresponding gold concentrations obtained

Figure 5

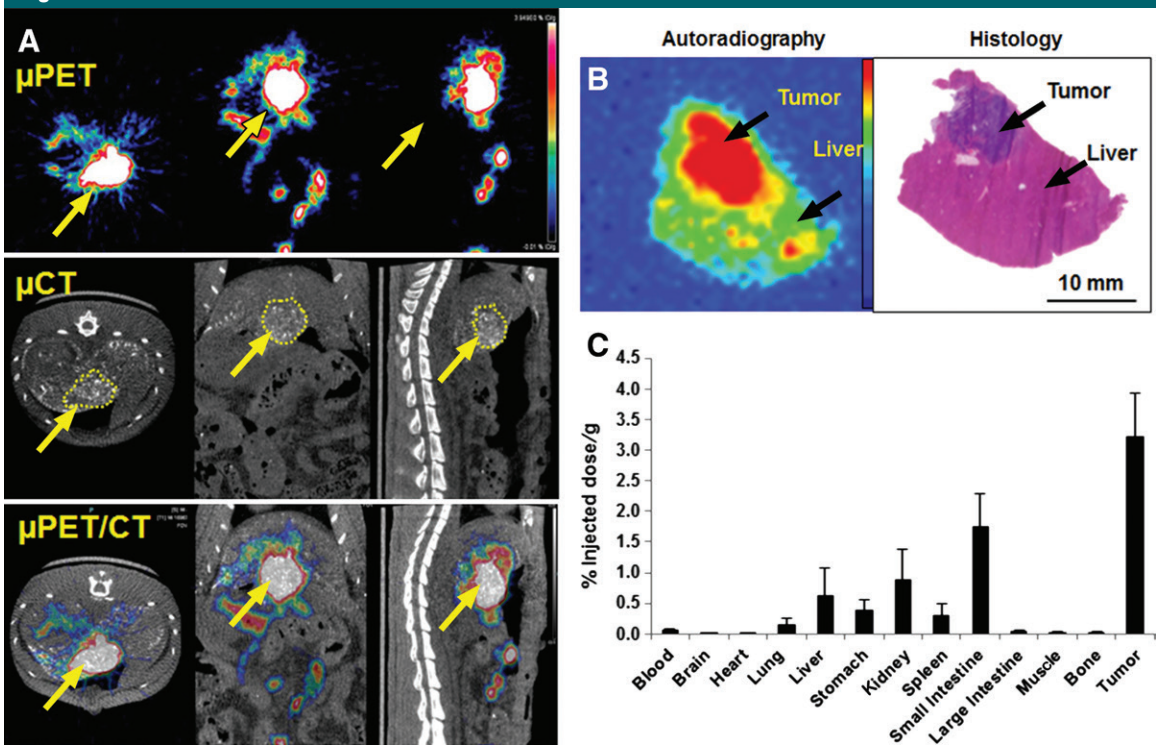

Figure 5: Micro-PET/CT *(μPET/CT)* images and biodistribution of PEG-[^{64}Cu]-HAuNS after intrahepatic arterial injection with CA4P. *A*, Areas of high radioactivity in N1S1 tumors (yellow arrows) on micro-PET images matched the contrast-enhanced regions on corresponding micro-CT images. *B*, Representative autoradiograph and microphotograph of hematoxylin and eosin–stained tumor and normal liver tissue. *C*, Bar graph shows biodistribution of PEG-[^{64}Cu]-HAuNS 1 hour after intrahepatic arterial injection after CA4P. Data are means ± standard deviation ($n = 5$).

Figure 6

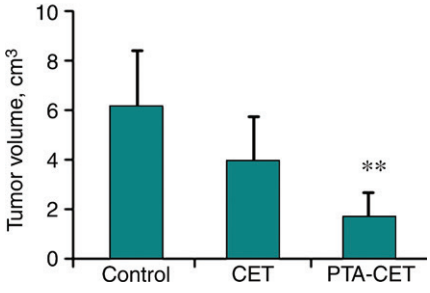

Figure 6: Graph shows therapeutic efficacy. Ten days after treatment, tumor volumes in PTA-CET group were significantly smaller than those in control and CET groups. ** = $P < .05$ compared with other groups.

from neutron activation analysis suggests that micro-CT of the tumor after intrahepatic arterial injection of PEG-HAuNS and ethiodized oil can be used as a surrogate to estimate tumor uptake of PEG-HAuNS. Our findings also indicate that micro-PET/CT can be used to quantify the tumor uptake of PEG-(^{64}Cu)-HAuNS, to guide therapy planning for near-infrared laser exposure, and to predict treatment outcome. In addition to clearly delineating tumors, micro-PET/CT demonstrated the enhanced tumor uptake of radiolabeled PEG-HAuNS and a high tumor-to-liver ratio of nanoparticle uptake; findings were confirmed by means of autoradiography, histopathologic evaluation, and biodistribution analysis.

Our findings also demonstrate the feasibility of using Dox@PEG-HAuNS, ethiodized oil, and near-infrared irradiation to destroy HCC effectively. With near-infrared irradiation, the tumor temperature rapidly increased to cell-ablative levels, whereas the adjacent liver temperature increased only slightly and remained within the safe range. Combined dark-field and fluorescence imaging allowed detection of both PEG-HAuNS and free Dox in areas of treated tumor 24 hours after near-infrared irradiation, indicating that near-infrared irradiation triggered the release of Dox from Dox@PEG-HAuNS. The combined PTA-chemotherapy had an enhanced therapeutic effect, as shown by significantly delayed tumor growth, which was supported by histopathologic results.

A few limitations of the current study should be noted. First, the released free Dox was expected to eliminate residual tumor cells not killed by PTA. However, this was not assessed in our study, and long-term studies are needed to assess the effect of released free Dox and local PTA on the elimination of remnant tumor cells and prevention of tumor regrowth. Second, in the management of HCC, controlling injury to normal liver parenchyma is as important as enhancing antitumor efficacy. More thorough studies are needed

to evaluate potential hepatotoxicity caused by PTA-CET. Third, additional treatment groups (eg, PEG-HAuNS, ethiodized oil, and near-infrared laser; CA4P, PEG-HAuNS, ethiodized oil, and near-infrared laser) must be included to fully assess the role of CA4P and laser in the absence of Dox in the antitumor effect of PTA-CET. Finally, increasing the number of studied animals should decrease the error bar of the results and improve the statistical power.

Our findings have several important potential implications for patient care, providing that this technique can be translated to humans. First, Dox@PEG-(^{64}Cu)-HAuNS can facilitate PET-guided PTA-CET. Second, micro-CT, rather than real-time digital subtraction angiography, can be used to assess tumor uptake of intrahepatic arterially injected Dox@PEG-HAuNS and ethiodized oil. Third, CA4P pretreatment can prolong the retention of a relatively high concentration PEG-HAuNS or Dox@PEG-HAuNS inside the tumor, thus potentiating the antitumor effect of PTA and PTA-CET.

Acknowledgment: We thank Joseph Munch, BA, for editing the manuscript.

Disclosures of Conflicts of Interest: J.L. disclosed no relevant relationships. **M.Z.** disclosed no relevant relationships. **F.L.** disclosed no relevant relationships. **C.X.** disclosed no relevant relationships. **W.W.** disclosed no relevant relationships. **Q.C.** disclosed no relevant relationships. **X.W.** disclosed no relevant relationships. **J.D.R.** disclosed no relevant relationships. **X.J.** disclosed no relevant relationships. **Y.A.W.** disclosed no relevant relationships. **S.G.** disclosed no relevant relationships. **C.L.** disclosed no relevant relationships.

References

1. Schwartz M, Roayaie S, Konstadoulakis M. Strategies for the management of hepatocellular carcinoma. Nat Clin Pract Oncol 2007;4(7):424–432.
2. Llovet JM, Schwartz M, Mazzaferro V. Resection and liver transplantation for hepatocellular carcinoma. Semin Liver Dis 2005;25(2):181–200.
3. You J, Zhang G, Li C. Exceptionally high payload of doxorubicin in hollow gold nanospheres for near-infrared light-triggered drug release. ACS Nano 2010;4(2):1033–1041.
4. You J, Zhang R, Xiong C, et al. Effective photothermal chemotherapy using doxorubicin-loaded gold nanospheres that target EphB4 receptors in tumors. Cancer Res 2012;72(18):4777–4786.
5. You J, Zhang R, Zhang G, et al. Photothermal-chemotherapy with doxorubicin-loaded hollow gold nanospheres: A platform for near-infrared light-trigged drug release. J Control Release 2012;158(2):319–328.
6. Mahnken AH, Pereira PL, de Baère T. Interventional oncologic approaches to liver metastases. Radiology 2013;266(2):407–430.
7. Li L, ten Hagen TL, Bolkestein M, et al. Improved intratumoral nanoparticle extravasation and penetration by mild hyperthermia. J Control Release 2013;167(2):130–137.
8. Jokerst JV, Lobovkina T, Zare RN, Gambhir SS. Nanoparticle PEGylation for imaging and therapy. Nanomedicine (Lond) 2011;6(4):715–728.
9. Nichols JW, Bae YH. Odyssey of a cancer nanoparticle: from injection site to site of action. Nano Today 2012;7(6):606–618.
10. Lorusso PM, Boerner SA, Hunsberger S. Clinical development of vascular disrupting agents: what lessons can we learn from ASA404? J Clin Oncol 2011;29(22):2952–2955.
11. Siemann DW, Horsman MR. Vascular targeted therapies in oncology. Cell Tissue Res 2009;335(1):241–248.
12. Woods JA, Hadfield JA, Pettit GR, Fox BW, McGown AT. The interaction with tubulin of a series of stilbenes based on combretastatin A-4. Br J Cancer 1995;71(4):705–711.
13. Dark GG, Hill SA, Prise VE, Tozer GM, Pettit GR, Chaplin DJ. Combretastatin A-4, an agent that displays potent and selective toxicity toward tumor vasculature. Cancer Res 1997;57(10):1829–1834.
14. Lu W, Xiong C, Zhang G, et al. Targeted photothermal ablation of murine melanomas with melanocyte-stimulating hormone analog-conjugated hollow gold nanospheres. Clin Cancer Res 2009;15(3):876–886.
15. Tian M, Lu W, Zhang R, et al. Tumor uptake of hollow gold nanospheres after intravenous and intra-arterial injection: PET/CT study in a rabbit VX2 liver cancer model. Mol Imaging Biol 2013;15(5):614–624.
16. You J, Zhou J, Zhou M, et al. Pharmacokinetics, clearance, and biosafety of polyethylene glycol-coated hollow gold nanospheres. Part Fibre Toxicol 2014;11:26.
17. Guo Y, Klein R, Omary RA, Yang GY, Larson AC. Highly malignant intra-hepatic metastatic hepatocellular carcinoma in rats. Am J Transl Res 2010;3(1):114–120.
18. Li J, Sun Z, Zhang J, et al. A dual-targeting anticancer approach: soil and seed principle. Radiology 2011;260(3):799–807.
19. Ng QS, Mandeville H, Goh V, et al. Phase Ib trial of radiotherapy in combination with combretastatin-A4-phosphate in patients with non-small-cell lung cancer, prostate adenocarcinoma, and squamous cell carcinoma of the head and neck. Ann Oncol 2012;23(1):231–237.
20. Murata R, Overgaard J, Horsman MR. Combretastatin A-4 disodium phosphate: a vascular targeting agent that improves that improves the anti-tumor effects of hyperthermia, radiation, and mild thermoradiotherapy. Int J Radiat Oncol Biol Phys 2001;51(4):1018–1024.
21. Martinelli M, Bonezzi K, Riccardi E, et al. Sequence dependent antitumour efficacy of the vascular disrupting agent ZD6126 in combination with paclitaxel. Br J Cancer 2007;97(7):888–894.
22. Wang ES, Pili R, Seshadri M. Modulation of chemotherapeutic efficacy by vascular disrupting agents: optimizing the sequence and schedule. J Clin Oncol 2012;30(7):760–761; author reply 761–763.
23. Tozer GM, Prise VE, Wilson J, et al. Mechanisms associated with tumor vascular shut-down induced by combretastatin A-4 phosphate: intravital microscopy and measurement of vascular permeability. Cancer Res 2001;61(17):6413–6422.
24. Wang H, Sun X, Chen F, et al. Treatment of rodent liver tumor with combretastatin a4 phosphate: noninvasive therapeutic evaluation using multiparametric magnetic resonance imaging in correlation with microangiography and histology. Invest Radiol 2009;44(1):44–53.
25. Li J, Cona MM, Chen F, et al. Exploring theranostic potentials of radioiodinated hypericin in rodent necrosis models. Theranostics 2012;2(10):1010–1019.
26. Gao M, Yao N, Huang D, et al. Trapping effect on a small molecular drug with vascular-disrupting agent CA4P in rodent H22 hepatic tumor model: in vivo magnetic resonance imaging and postmortem inductively coupled plasma atomic emission spectroscopy. J Drug Target 2015;23(5):436–443.